TABLE VI. Summary of main structure in the calculated $\epsilon_{2\perp}(\omega)$ for SnS$_2$ and the measured reflectivity.

Structure in reflectivity (eV)	Structure in $\epsilon_{2\perp}(\omega)$ (eV)	Identification main transitions
3.8	3.9	M_0 $\Gamma_{3'} \to \Gamma_1$
	4.0	Volume effect $7 \to 9$, $8 \to 9$
4.9	4.9	Volume effect $6 \to 9$, $7 \to 9$, $8 \to 9$
	5.4	$6 \to 9$, $7 \to 9$, $7 \to 10$, $8 \to 10$
5.8	5.7	$6 \to 9$, $7 \to 9$, $7 \to 10$, $8 \to 10$
6.9	6.8	$6 \to 10$, $7 \to 10$, $8 \to 10$, $7 \to 11$, $8 \to 11$

the experimental reflectivity[5] curve with structure at 3.8, 4.9, 5.8, and 6.9 eV. There is no experimental optical data for SnS$_2$ with light polarized along the $\vec{c}$ axis. We summarize the structure in $\epsilon_2(\omega)$ and the measured reflectivity in Table VI.

*Work supported in part by the National Science Foundation under Grant No. 13632.

[1]See for example, J. A. Wilson and A. D. Yoffe, Advan. Phys. 18, 193 (1969).

[2]E. Mooser and W. B. Pearson, Phys. Rev. 101, 492 (1956).

[3]G. Busch, C. Frohlich, and F. Hulliger, Helv. Phys. Acta 34, 359 (1961).

[4]S. Asanabe, J. Phys. Soc. Japan 16, 1789 (1961).

[5]D. L. Greenway and R. Nitsche, J. Phys. Chem. Solids 26, 1445 (1965).

[6]G. Domingo, R. S. Itoga, and C. R. Kannewurf, Phys. Rev. 143, 536 (1966).

[7]P. A. Lee and G. Said, J. Phys. 1, 837 (1968).

[8]M. Y. Au-Yang and M. L. Cohen, Phys. Rev. 178, 1279 (1969).

[9]R. W. G. Wyckoff, Crystal Structure, 2nd ed. (Interscience, New York, 1963), p. 266.

[10]M. Tinkham, Group Theory and Quantum Mechanics (McGraw-Hill, New York, 1964), p. 53.

[11]See, for example, A. W. Luehrmann, Ph.D. thesis (University of Chicago, 1967) (unpublished).

[12]M. L. Cohen and T. K. Bergstresser, Phys. Rev. 141, 789 (1966).

[13]D. Brust, Phys. Rev. 134, A1337 (1964).

[14]A. O. E. Aminalu and V. Heine, Phil. Mag. 12, 1249 (1965).

[15]J. P. Walter and M. L. Cohen, Phys. Rev. 183, 763 (1969).

[16]R. N. Cahn and M. L. Cohen, Phys. Rev. B 1, 2569 (1970).

Frequency- and Wave-Vector-Dependent Dielectric Function for Silicon†

John P. Walter* and Marvin L. Cohen

*Department of Physics, University of California and Inorganic Materials Research Division,
Lawrence Radiation Laboratory, Berkeley, California 94720*

(Received 15 November 1971)

The frequency- and wave-vector-dependent complex dielectric function $\epsilon(\vec{q}, \omega)$ is calculated for silicon. The energy eigenvalues and eigenvectors which are used have been obtained from energy-band calculations based on the empirical pseudopotential method. Explicit results are given in the [100] direction in the range $0 \le q \le (2\pi/a)$ and $0 \le \hbar\omega \le 24$ eV. A comparison is made between the present results and the results of a calculation of $\epsilon(q, \omega)$ for a free-electron gas in the random-phase approximation.

I. INTRODUCTION

We have calculated the frequency- and wave-vector-dependent dielectric function $\epsilon(\vec{q}, \omega)$ in the [100] direction for silicon. This is the first calculation of $\epsilon(\vec{q}, \omega)$ for a semiconductor in which realistic energy eigenvalues and eigenvectors are used. Previous calculations of dielectric functions have concentrated either on the wave-vector-de-

pendent dielectric function[1] for zero frequency $\epsilon(\vec{q}, \omega = 0)$ or on the frequency-dependent dielectric function[2] $\epsilon(\vec{q} = 0, \omega)$. The former case is important in determining the static screening of electric fields, and the latter case is important in analyzing the optical properties of semiconductors because q is approximately zero for optical wave vectors. The more general dielectric function $\epsilon(\vec{q}, \omega)$ describes the screening of a longitudinal field which

varies in both space and time. A knowledge of $\epsilon(\vec{q}, \omega)$ permits us to obtain the following properties of the solid: the response to weak external longitudinal fields, the density-fluctuation excitation spectrum (energy loss of a fast charged particle), and the time-dependent correlations between the density fluctuations (plasmon modes).

In the present calculation the real part of the dielectric function $\epsilon_1(\vec{q}, \omega)$ is calculated directly, and the imaginary part $\epsilon_2(\vec{q}, \omega)$ is calculated using the Kramers-Krönig transformation. The functions $\epsilon_1(\vec{q}, \omega)$ and $\epsilon_2(\vec{q}, \omega)$ are then used to calculate the imaginary part of the inverse dielectric function $\mathrm{Im}\,\epsilon^{-1}(\vec{q}, \omega)$, which is proportional, for small q, to the energy-loss function of a fast charged particle passing through the solid.

The details of the calculation are given in Sec. II along with the results for silicon. In Sec. III the silicon calculations are compared with a calculation of $\epsilon_1(q, \omega)$, $\epsilon_2(q, \omega)$, and $\mathrm{Im}\,\epsilon^{-1}(q, \omega)$ for a free-electron gas in the random-phase approximation, that is, the Lindhard[3] dielectric function. A comparison of the various dielectric functions for silicon and the free-electron gas illustrates the principal difference between the two cases.

II. CALCULATIONS

First we calculate the longitudinal wave-vector-dependent and frequency-dependent dielectric function $\epsilon(\vec{q}, \omega)$ for silicon which describes the response of a crystal to an electric field parallel to $\vec{q}$ and varying sinusoidally in time:

$$\vec{D}\,e^{i(\vec{q}\cdot\vec{r}-\omega t)} = \epsilon(\vec{q}, \omega)\,\vec{E}\,e^{i(\vec{q}\cdot\vec{r}-\omega t)} . \tag{2.1}$$

Using the expression for $\epsilon_1(\vec{q}, \omega)$ given by Ehrenreich and Cohen,[4] we obtain

$$\epsilon_1(\vec{q}, \omega) = 1 + \frac{4\pi e^2}{\Omega q^2} \sum_{\vec{k},c,v} |\langle \vec{k}, c | \vec{k}+\vec{q}, v \rangle|^2$$

$$\times \{ [E_c(\vec{k}) - E_v(\vec{k}+\vec{q}) - \hbar\omega]^{-1}$$

$$+ [E_c(\vec{k}) - E_v(\vec{k}+\vec{q}) + \hbar\omega]^{-1} \} , \tag{2.2}$$

where $\vec{k}$ is summed over the first Brillouin zone, v labels the valence bands, and c labels the conduction bands. For the purposes of calculation, Eq. (2.2) is written as follows

$$\epsilon_1(\vec{q}, \omega) = 1 + \frac{4\pi e^2}{q^2} \frac{2}{(2\pi)^3} \sum_{\Delta k,c,v} |\langle \vec{k}, c | \vec{k}+\vec{q}, v \rangle|^2 (\Delta k)^3$$

$$\times \{ [E_c(\vec{k}) - E_v(\vec{k}+\vec{q}) - \hbar\omega]^{-1}$$

$$+ [E_c(\vec{k}) - E_v(\vec{k}+\vec{q}) + \hbar\omega]^{-1} \} , \tag{2.3}$$

where the summation is over cubes of volume $(\Delta k)^3$ in the first Brillouin zone, with suitable truncations at the zone boundaries. The summation index v spans the top-four valence bands and the index c spans the bottom-eleven conduction bands. $E_n(\vec{k})$

is the energy eigenvalue of band n at state $\vec{k}$, and $|\vec{k}, n\rangle$ is the corresponding eigenvector.

The energy eigenvalues and eigenvectors are calculated using the empirical pseudopotential method, as described in Ref. 2. Since spin-orbit effects are small for silicon, they have not been included in this calculation. The pseudopotential form factors have been adjusted so that the reflectivity and the principal optical gaps agree with experimental measurements.[5,6] Fifteen energy eigenvalues and eigenvectors are computed for each of 3360 points in the Brillouin zone. The coordinates of the grid of calculated points are given by $\frac{1}{16}(2s+1, 2m+1, 2n+1)$ in units of $2\pi/a$, where s, m, and n are integers.

For an arbitrary direction of $\vec{q}$, the summation in Eq. (2.3) must be performed over the entire Brillouin zone. Fortunately, symmetry properties can be exploited to reduce the computation time by a factor of 8 in the [100] direction. The computation time for a particular value of $\vec{q}$ can be reduced by an additional factor of 15 if $\vec{q}$ is chosen such that $(\vec{k}+\vec{q})$ also lies on the grid of calculated points.

For certain values of $c, v, \vec{k}, \vec{q}$, and ω, $[E_c(\vec{k}) - E_v(\vec{k}+\vec{q}) - \hbar\omega]^{-1}$ can have singularities and it varies rapidly as $\vec{k}$ varies over the cube of volume $(\Delta k)^3$. For such cases, the cube is divided into 216 equal subcubes. The contributions of $(E_c - E_v - \hbar\omega)^{-1}$ are calculated by interpolation and are added together and multiplied by the new volume of $(\Delta k)^3/216$. The values of $|\langle \vec{k}, c | \vec{k}+\vec{q}, v \rangle|^2$ and $[E_c(\vec{k}) - E_v(\vec{k}) + \hbar\omega]^{-1}$, which are not singular, vary much more slowly and are given the values they assume at the center of the larger cubes.

An indication of the accuracy of the present calculation of $\epsilon_1(q=0, \omega)$ is given by a comparison with a much more accurate calculation done in conjunction with the work on silicon presented in Ref. 6. In this previous calculation, 356 points in $\frac{1}{48}$ of the Brillouin zone were accurately computed and then the energy eigenvalues and the dipole matrix elements were both determined on a much finer grid of 175 000 points in $\frac{1}{48}$ of the Brillouin zone by means of an interpolation scheme. The comparison in Fig. 1 shows that the present calculation of $\epsilon_1(\vec{q}=0, \omega)$ is approximately correct, and this, in turn, indicates the accuracy of our calculations of $\epsilon(\vec{q}, \omega)$.

After we calculate $\epsilon_1(\vec{q}, \omega)$, the imaginary part of the dielectric function $\epsilon_2(\vec{q}, \omega)$ is calculated by a Kramers-Krönig transform of $\epsilon_1(\vec{q}, \omega)$. The imaginary part of the inverse dielectric function $\mathrm{Im}\,\epsilon^{-1}(\vec{q}, \omega)$ is then easily computed. Figures 2–6 display plots of $\epsilon_1(\vec{q}, \omega)$, $\epsilon_2(\vec{q}, \omega)$, and $\mathrm{Im}\,\epsilon^{-1}(\vec{q}, \omega)$ as a function of ω for $q=0$, $\frac{1}{4}$, $\frac{1}{2}$, $\frac{3}{4}$, and 1 in units of $2\pi/a$ in the [100] direction. In Ref. 1 we have shown that $\epsilon_1(\vec{q}, \omega=0)$ is nearly isotropic with only minor deviations for $\vec{q}$ parallel to the [111] direc-
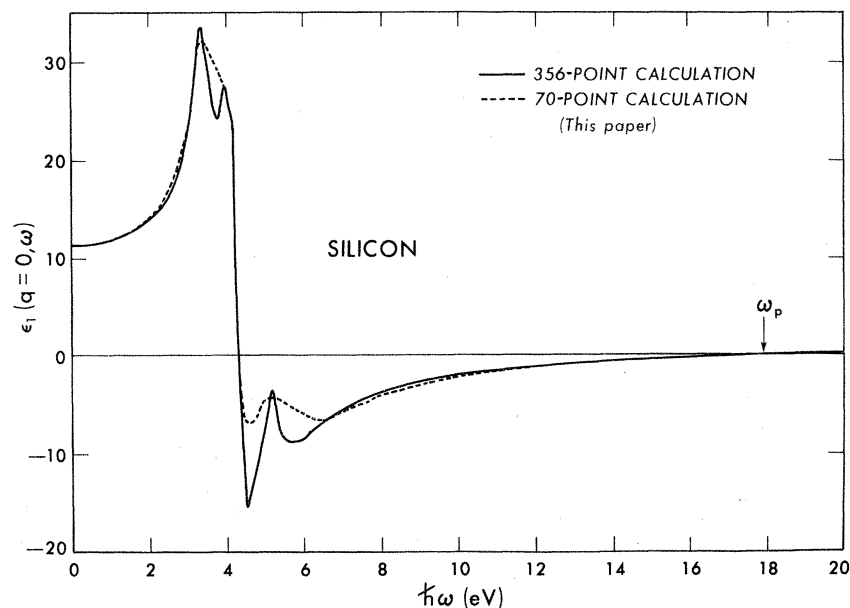
tion. Therefore, we expect that $\epsilon(\vec{q},\omega)$ does not change significantly in shape for other directions of $\vec{q}$.

The numerical accuracy of the Kramers-Krönig transform is excellent; however, the reader should notice that $\epsilon_2(\vec{q},\omega)$ is negative for $q=0,\frac{1}{4}$, for small
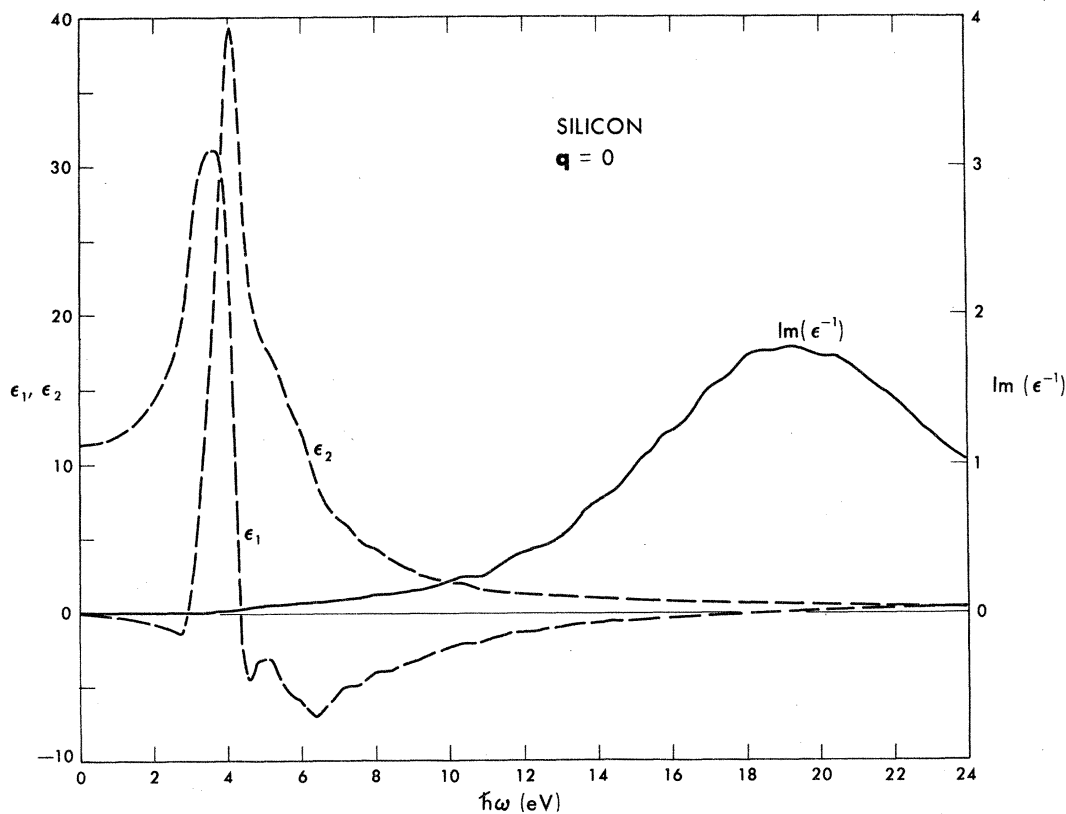

FIG. 2. Plots of ϵ_1, ϵ_2, and Imϵ^{-1} for silicon as a function of $\hbar\omega$ for $\vec{q}=(0,0,0)$.

ω, whereas it should be zero because of the energy gap. This incorrect result is caused by small errors in the calculation of $\epsilon_1(\vec{q}, \omega)$. Small errors in ϵ_1 and ϵ_2 can cause larger errors in $\mathrm{Im}\epsilon^{-1}$, and for this reason the smaller structure in the plots of $\mathrm{Im}\epsilon^{-1}$ is not to be regarded as accurate.

III. DISCUSSION

In this section we compare the results for the silicon $\epsilon_1(\vec{q}, \omega)$, $\epsilon_2(\vec{q}, \omega)$, and the $\mathrm{Im}[\epsilon^{-1}(\vec{q}, \omega)]$ with these functions calculated for a free-electron gas in the random-phase approximation. This RPA, or Lindhard dielectric function, has the form

$$\epsilon_1(\beta, \delta) = 1 + \frac{K_S^2}{8\beta q^2}\left([1 - (\beta + \gamma)^2]\ln\left|\frac{1+\beta+\gamma}{1-\beta-\gamma}\right| + [1 - (\beta - \gamma)^2]\ln\left|\frac{1+\beta-\gamma}{1-\beta+\gamma}\right| + 4\beta \right) \tag{3.1}$$

and

$$\epsilon_2(\beta, \delta) = \frac{\pi K_S^2}{8\beta q^2}\times\begin{cases} \delta & \text{when } \beta < 1 \text{ and } \delta < |4\beta^2 - 4\beta| \\ [1 - (\beta - \gamma)^2]\text{ when } |4\beta^2 - 4\beta| < \delta < |4\beta^2 + 4\beta| \\ 0 & \text{when } \delta > |4\beta^2 + 4\beta| \\ 0 & \text{when } \beta > 1 \text{ and } \delta < |4\beta^2 - 4\beta| \end{cases} \tag{3.2}$$

where $\beta = q/2k_F$, $\delta = \hbar\omega/E_F$, $\gamma = \delta/4\beta$, K_S is the inverse Fermi-Thomas screening length, k_F is the free-electron Fermi wave vector, and E_F is the Fermi energy.

$\epsilon_1(\vec{q}, \omega)$ for silicon is displayed in a perspective plot (Fig. 7) which more clearly illustrates how ϵ_1 varies in the $(\vec{q}, \omega)$ plane. In Fig. 8 we give a similar plot of the Lindhard $\epsilon_1(q, \omega)$ obtained from evaluating Eq. (3.1) for a density of free electrons that give a plasma frequency ω_p identical to the

calculated silicon value. [The plasma frequency ω_p is given by the high-frequency zero of $\epsilon_1(\vec{q}, \omega)$].

For $q = 0$ and ω small, the silicon ϵ_1 and the Lindhard ϵ_1 differ markedly. In particular, the Lindhard ϵ_1 assumes the familiar form $\epsilon_1(q = 0, \omega) = 1 - \omega_p^2/\omega^2$, which has a singularity at $\omega = 0$. This is in complete contrast with the silicon ϵ_1, which is an increasing positive function for small ω. The significant difference between the two functions at $q = 0$ is that the lower zero of the silicon ϵ_1 occurs
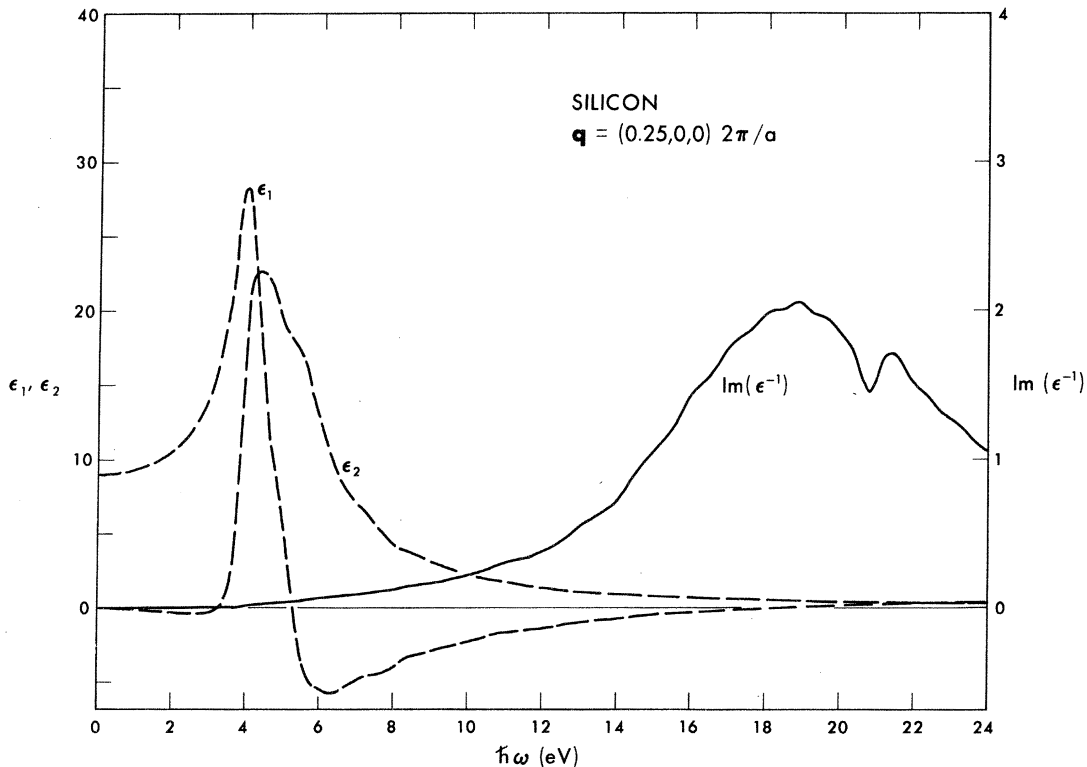

FIG. 3. Plots of ϵ_1, ϵ_2, and $\mathrm{Im}\epsilon^{-1}$ for silicon as a function of $\hbar\omega$ for $\vec{q} = (\frac{1}{4}, 0, 0)2\pi/a$.
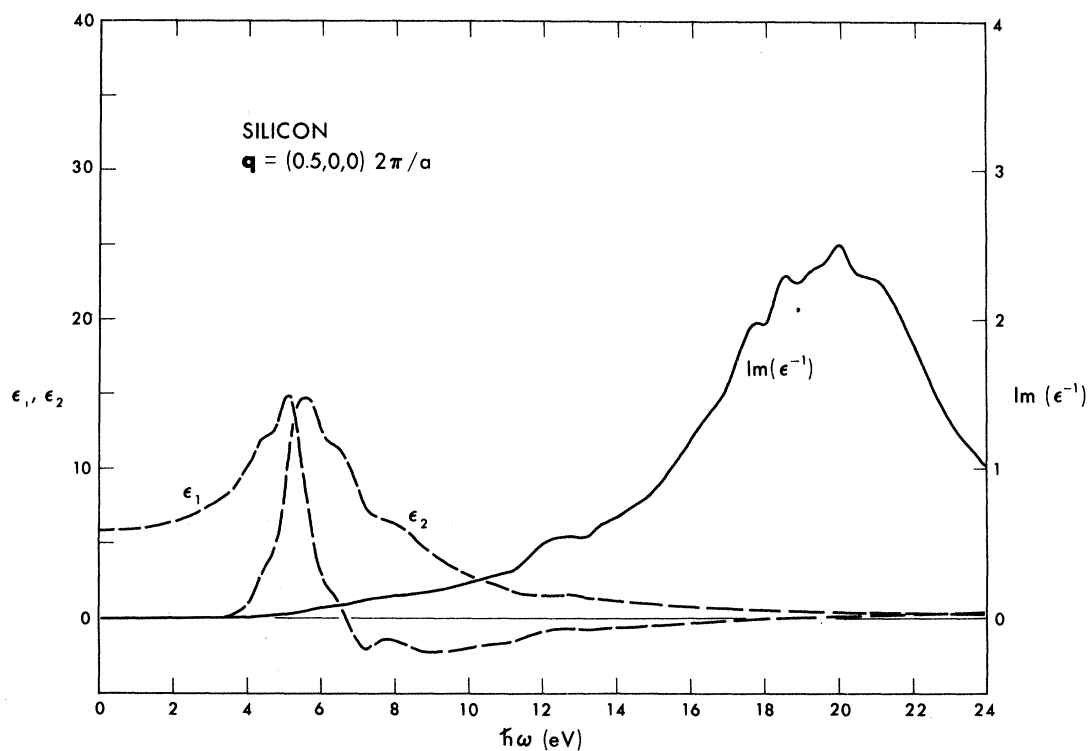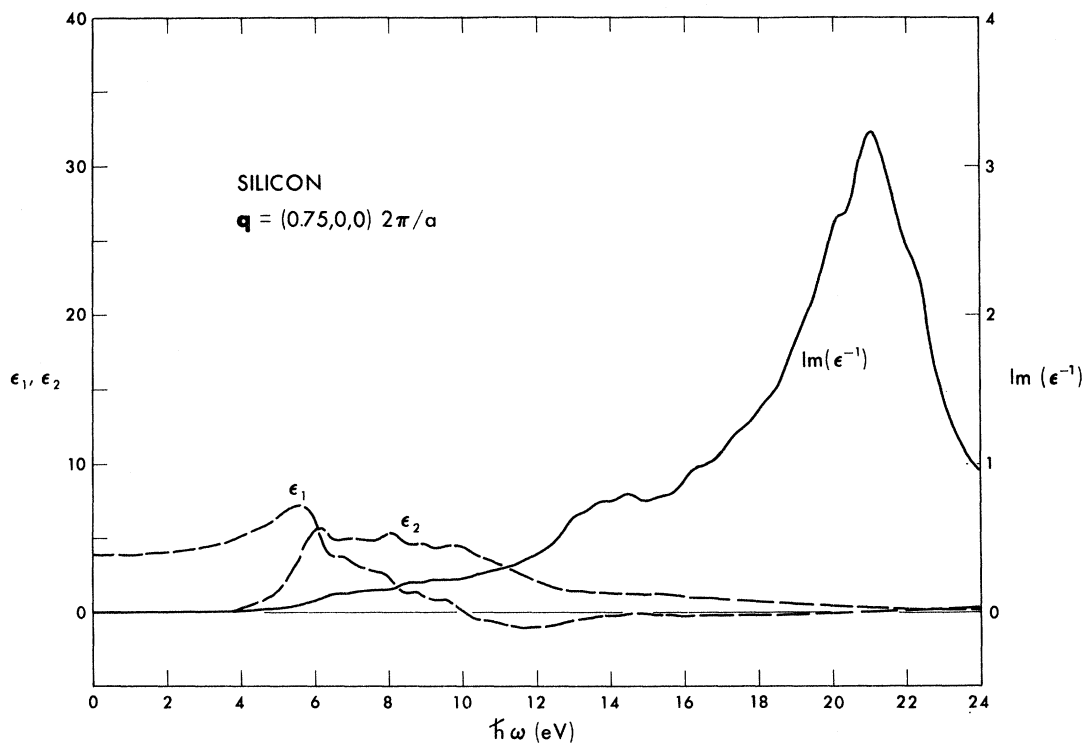
FIG. 4. Plots of ϵ_1, ϵ_2, and $\mathrm{Im}\,\epsilon^{-1}$ for silicon as a function of $\hbar\omega$ for $\vec{q} = (\frac{1}{2}, 0, 0)2\pi/a$.

FIG. 5. Plots of ϵ_1, ϵ_2, and $\mathrm{Im}\,\epsilon^{-1}$ for silicon as a function of $\hbar\omega$ for $\vec{q} = (\frac{3}{4}, 0, 0)2\pi/a$.
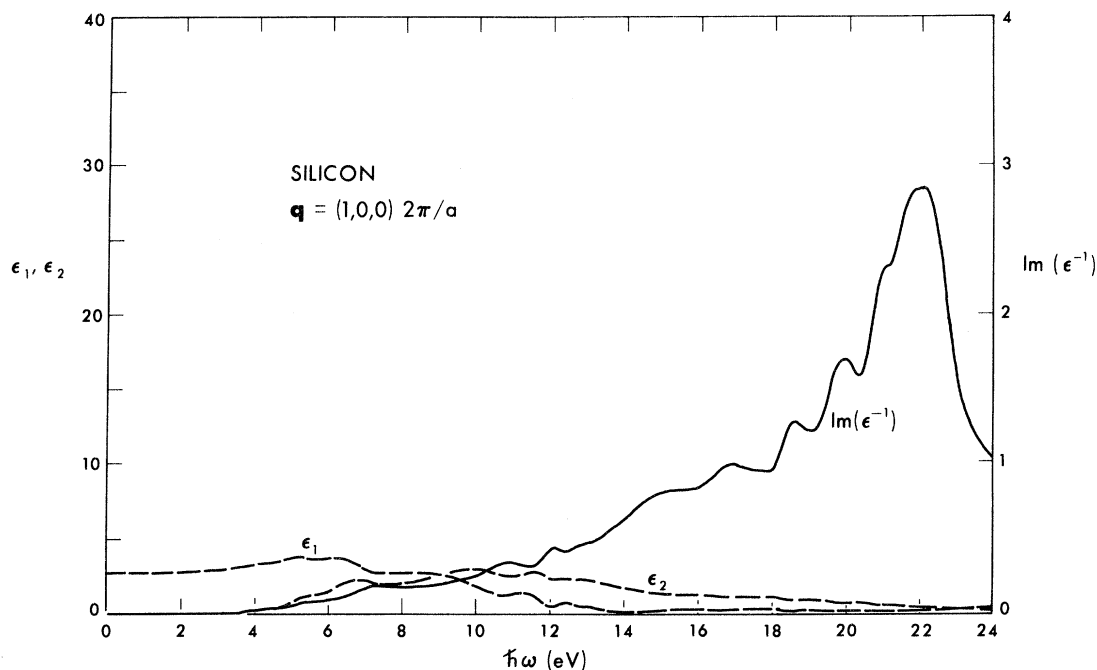
FIG. 6. Plots of ϵ_1, ϵ_2, and $Im\epsilon^{-1}$ for silicon as a function of $\hbar\omega$ for $\vec{q} = (1, 0, 0)2\pi/a$.

at about 4.5 eV, whereas the zero of the Lindhard ϵ_1 occurs at zero. The behavior of the lower zero in ϵ_1 is discussed later in greater detail. For small ω at all nonzero values of q, the silicon ϵ_1 increases with ω until the function reaches a maximum, but for the Lindhard case, ϵ_1 decreases with

increasing ω, so that the maximum value of the Lindhard ϵ_1 always occurs at $\omega = 0$.

At high ω for all q the silicon and Lindhard ϵ_1 functions are similar. This is reasonable, since at high ω (such that $\hbar\omega$ is much larger than the energy gap), we expect silicon to resemble a free-
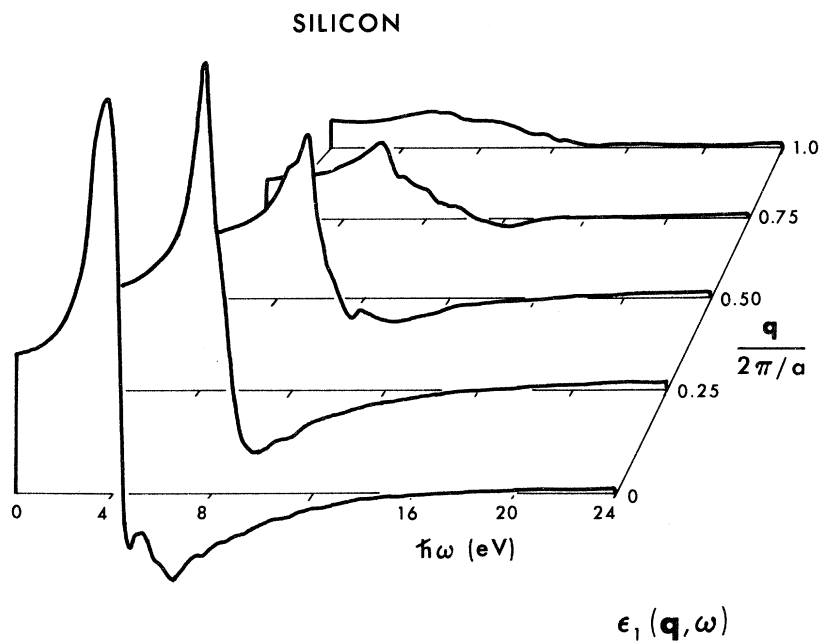

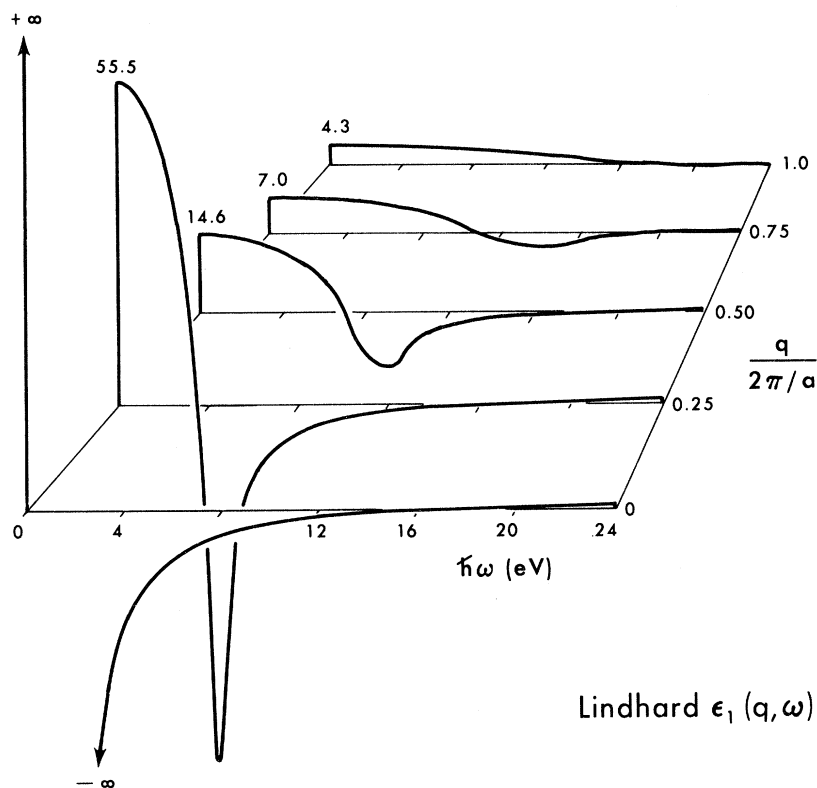FIG. 7. Perspective plot of $\epsilon_1(\vec{q}, \omega)$ for silicon.

FIG. 8. Perspective plot of $\epsilon_1(q, \omega)$ for a free-electron gas.

electron gas because the high-energy excited states correspond to loosely bound electrons.

In Figs. 9 and 10 $\epsilon_2(q, \omega)$ is plotted for the silicon and Lindhard cases. Because of the gap, the silicon ϵ_2 is identically zero at small ω, while in the Lindhard case ϵ_2 differs from zero for small ω for all q. The Lindhard $\epsilon_2(\omega)$ first increases linearly and then falls quadratically with ω for each q [see Eq. (3.2)]. The quadratic dependence is not clearly visible in Fig. 10 because of the per-
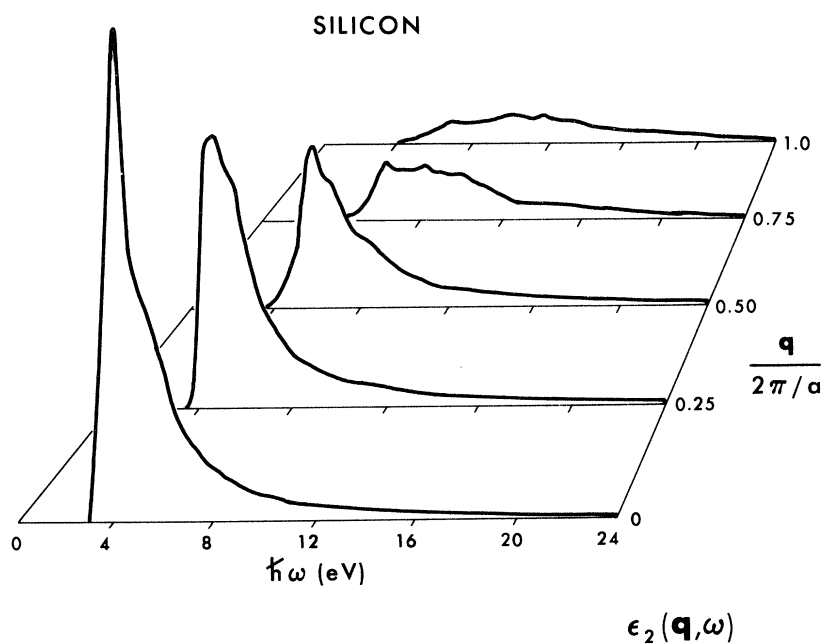

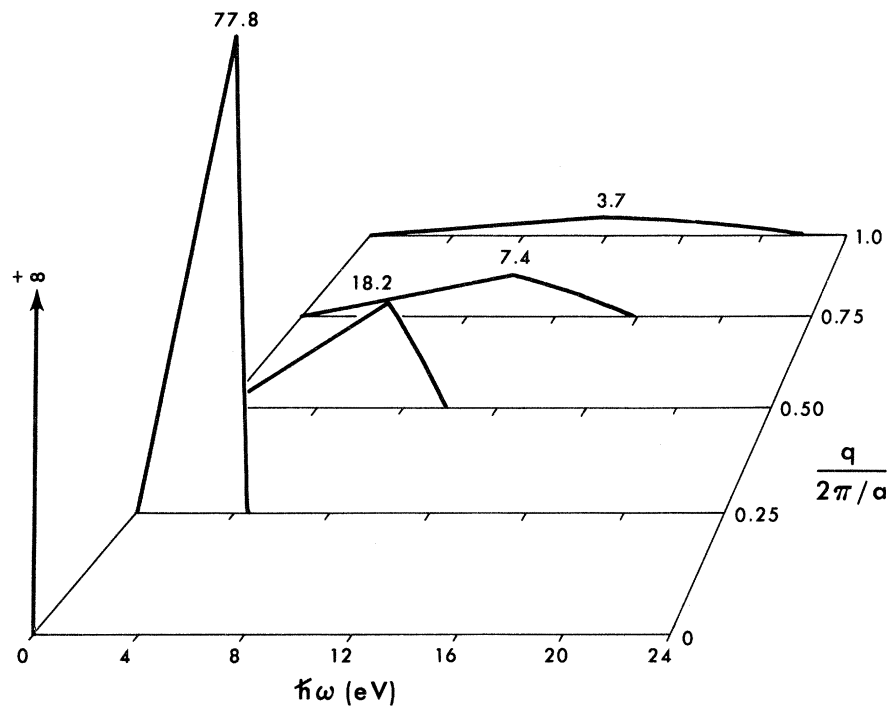FIG. 9. Perspective plot for $\epsilon_2(\vec{q}, \omega)$ for silicon.

Lindhard $\epsilon_2(q,\omega)$

FIG. 10. Perspective plot of $\epsilon_2(q, \omega)$ for a free-electron gas.

spective nature of the graph and the rapid depen-
dence of ϵ_2 on ω in these regions. As in the case
of $\epsilon_1(q, \omega)$, the differences in $\epsilon_2(q, \omega)$ between the

silicon and Lindhard cases are most prominent at
low q and ω.

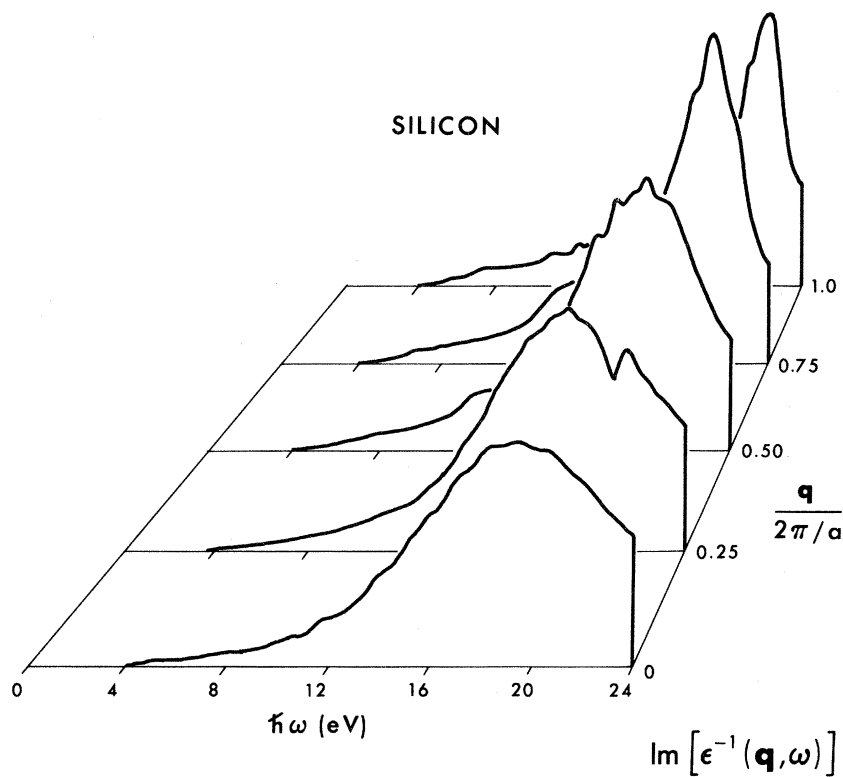Figures 11 and 12 show $\text{Im}[\epsilon^{-1}(\vec{q}, \omega)]$ for the

SILICON

$\text{Im}\left[\epsilon^{-1}(q,\omega)\right]$

FIG. 11. Perspective plot of
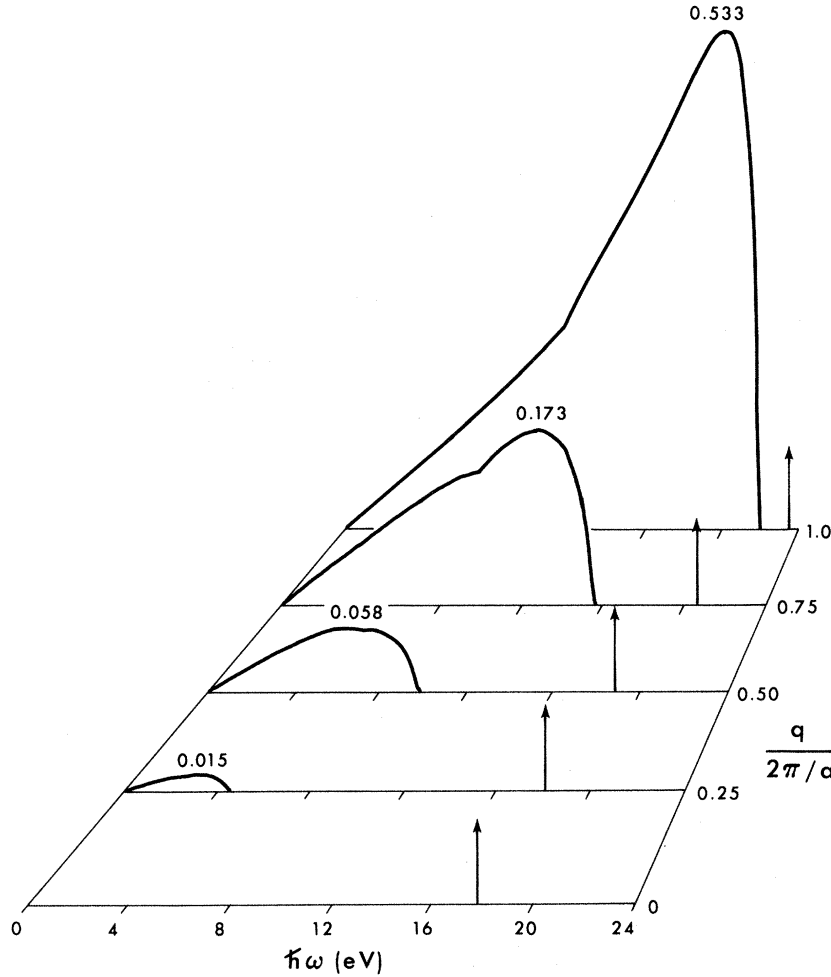$\text{Im}[\epsilon^{-1}(\vec{q}, \omega)]$ for silicon.

0.533

0.173

0.058

0.015

1.0

0.75

0.50

0.25

0

$\dfrac{q}{2\pi/a}$

0   4   8   12   16   20   24

$\hbar\omega$ (eV)

FIG. 12. Perspective plot of $\mathrm{Im}\,|\,\epsilon^{-1}(q,\omega)\,|$ for a free-electron gas. The arrows are δ functions.

Lindhard $\mathrm{Im}\left|\,\epsilon^{-1}(q,\omega)\,\right|$

silicon and Lindhard cases. These cases differ considerably. In the Lindhard case the function approaches zero as q and ω approach zero except for the characteristic δ function at $\omega = \omega_p$. It becomes finite and increases in magnitude as q and ω become larger. The sum rules are satisfied by appropriate contributions at $\omega_p(q)$. The function becomes finite for each nonzero q as ω increases from zero, whereas for silicon the gap in the ϵ_2 spectrum causes the $\mathrm{Im}[\epsilon^{-1}(q,\omega)]$ function to be zero at small ω. Comparison with experiment can be made with optical work[7] and electron-energy-loss measurements.[8] The agreement is good with respect to amplitude, width, and position of the peak, but we caution the reader against taking the small structure near ω_p seriously in Fig. 11. In this energy range ϵ_1 and ϵ_2 are close to zero, and small errors are magnified in the $\mathrm{Im}[\epsilon^{-1}(\vec{q},\omega)]$ function.

For the Lindhard case (Fig. 12), pair-excitation

(lower ω) contributions to $\mathrm{Im}[\epsilon^{-1}]$ eventually merge with the plasmon contribution at larger q. This occurs for q's where the $\omega(q)$ line satisfying $\epsilon_1[q,\omega(q)]=0$ enters the continuum. For the present case, this happens when $1.176 < qa/2\pi < 1.177$. The upper end of the spectrum is still sharply peaked resembling a plasmonlike contribution. For silicon (Fig. 11) this occurs even at $q = 0$, and the ϵ_2 coming from pair excitations damps the plasmon peak.

It is interesting to examine the q and ω dependence of the zeros of the $\epsilon_1(q,\omega)$ function in the (q,ω) plane. The results are given in Fig. 13. For the Lindhard case the lower zero ω_0 of ϵ_1 occurs at frequencies which are linear in q. This can be seen by expanding the Lindhard function given in Eq. (3.1) for small q and ω. An easier method is to use the precursor to Eq. (3.1):

$$\epsilon(\vec{q},\omega) = 1 + \frac{4\pi e^2}{q^2}\sum_{\vec{k}}' \frac{f(\vec{k}+\vec{q})-f(\vec{k})}{E(\vec{k}+\vec{q})-E(\vec{k})-\hbar\omega} \quad . \qquad (3.3)$$
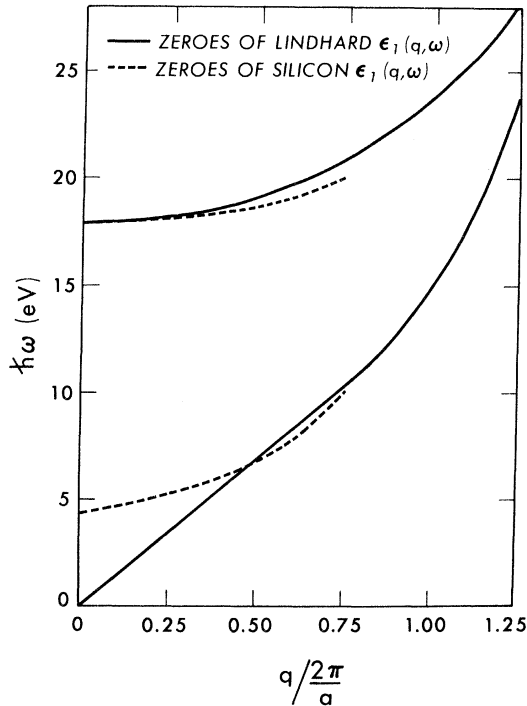
FIG. 13. Plots of the zeros of $\epsilon_1(\vec{q}, \omega)$ for silicon and a free-electron gas in the $(\vec{q}, \omega)$ plane.

For small q, the difference in the Fermi factors becomes

$$f(\vec{k}+\vec{q}) - f(\vec{k}) \approx \vec{q} \cdot \frac{\partial f}{\partial \vec{k}} \approx q\mu\delta(k - k_F) , \qquad (3.4)$$

where

$$\mu = \vec{k} \cdot \vec{q}/kq .$$

Dropping terms in q^2 in the integrand, the dielectric function becomes

$$\epsilon(q, \omega) = 1 + \frac{K_s^2}{2q^2} \int_{-1}^{1} \frac{\mu d\mu}{\mu - \gamma} = 1 + \frac{K_s^2}{2q^2}\left(2 - \gamma \ln\left|\frac{1+\gamma}{1-\gamma}\right| \right),$$
$$(3.5)$$

where $\gamma = \omega/qv_F$. The lower zero (which looks like a damped transverselike mode in the continuum) arises when

$$2 \approx \gamma \ln\left| (1+\gamma)/(1-\gamma) \right| . \qquad (3.6)$$

This condition requires a fairly linear $\omega(q)$ curve, i.e.,

$$\omega \approx \tfrac{5}{6} v_F q , \qquad (3.7)$$

which agrees well with the computer calculations.

For silicon the lower zero does not result from a linear dispersion curve, but a gap appears in the spectrum. This is the most significant difference between the two dielectric functions. At higher q, the two curves tend to merge, but it is more difficult to calculate the zeros of ϵ_1 in this region of the plane. In other words, it is the gap in the spectrum at smaller q which distinguishes the silicon case from the free-electron-gas case as expected.

ACKNOWLEDGMENT

*Present address: Department of Physics, Brandeis University, Waltham, Mass. 02154.

[1]J. P. Walter and M. L. Cohen, Phys. Rev. B 2, 1821 (1970).

[2]M. L. Cohen and V. Heine, Solid State Phys. 24, 37 (1970).

[3]J. Lindhard, Kgl. Danske Videnskab Selskab, Mat.-Fys. Medd. 28, 8 (1954).

[4]H. Ehrenreich and M. H. Cohen, Phys. Rev. 115, 786 (1959).

[5]D. Brust, M. L. Cohen, and J. C. Phillips, Phys. Rev. Letters 9, 389 (1962).

[6]R. R. L. Zucca, J. P. Walter, Y. R. Shen, and M. L. Cohen, Solid State Commun. 8, 627 (1970).

[7]H. R. Philipp and H. Ehrenreich, Phys. Rev. 129, 1550 (1963).

[8]H. Dimigen, Z. Physik 165, 53 (1961).